Combined shearlet and TV regularization in sparse-view CT reconstruction

Bert Vandeghinste, Bart Goossens, Roel Van Holen, Christian Vanhove, Aleksandra Pižurica,
Stefaan Vandenberghe and Steven Staelens

Abstract—Preclinical in vivo micro computerized tomography suffers from high image noise, due to limitations on total scanning time and the small pixel sizes. A lot of different noise minimization algorithms have already been proposed to reconstruct images acquired in low dose settings. Sparse-view reconstruction amongst others can reduce acquisition dose significantly, by acquiring only a small subset of projection views. Total Variation minimization has been used extensively to solve these problems. However, the performance of TV is suboptimal for complex images, compared to simple images with little texture. This is mainly due to the underlying piecewise constant image model imposed by TV.

A recent efficient solver was developed for convex problems, able to incorporate regularization terms different from TV. The work presented here is a proof-of-concept study combining both TV as well as shearlets as regularization terms into one general CT reconstruction algorithm. Shearlets, closely related to wavelets, take edges into account in a multitude of directions at different scales, and have good compaction properties. This makes shearlets a better candidate than TV for compressed sensing problems. The resulting reconstructions were compared to TV minimization and to shearlet minimization. The combination of both shows benefits for sparse-view CT imaging, and leads to edge-preserved image denoising. Difference images show a very small loss in resolution, which may be caused by difficult parameter selection.

Index Terms—Computed Tomography, Iterative Algorithms, Noise, Reconstruction Algorithms

I. INTRODUCTION

Preclinical in vivo micro computerized tomography (μCT) suffers from high image noise, as a result of the small detector pixel sizes, a high scatter-to-primary noise ratio [1], and the limited time animals can be safely kept under anesthetics. This results in limited soft tissue contrast. Reducing the dose without sacrificing image quality could offer significant benefits for longitudinal preclinical research, where the small animals receive a large dose within a timeframe of several days to weeks.

*B. Vandeghinste, R. Van Holen, C. Vanhove, S. Vandenberghe and S. Staelens are with the Medical Image and Signal Processing (MEDISIP) research group, Ghent University–IBBT, 9000 Gent, Belgium. (e-mail: bert.vandeghinste@ugent.be).

B. Goossens and A. Pižurica are with the Image Processing and Interpretation (IPI) research group, Ghent University–IBBT, Sint-Pietersnieuwstraat 41, 9000 Gent, Belgium.

S. Staelens is also with the Molecular Imaging Centre Antwerp, University of Antwerp, 2650 Edegem, Belgium.

Total variation (TV) minimization has been extensively investigated in the last decade for image denoising in general and sparse-view reconstruction in particular [2]–[5]. These methods have been shown to have superior denoising performance in simple classes of images. However, TV minimization produces cartoon-like approximations due to its underlying image model. This model biases the results towards distorted images, which may be less suitable for medical images used in diagnostics [3].

In the search for objective functions different from TV, a recent efficient solver was developed, based on a split-Bregman approach. With this solver, other regularization terms can easily be tested. One possibility is the shearlet [6], [7], closely related to wavelets, which has better directional sensitivity, better ℓ_1-norm sparsity and, because of a different underlying image model, does not lead to the staircasing effect. We have previously shown that shearlet-regularized reconstructed images show no staircasing and exhibit small aliasing artifacts. However, these reconstructions did not outperform TV-based regularization for all datasets [8]. In the research presented here, we investigated if combining TV and shearlets can combine their benefits and reduce the small artifacts induced by using shearlets in CT reconstruction. This combination has already been shown effective in Magnetic Resonance Imaging reconstruction [9]–[11].

The remainder of this paper is organized as follows. In Sec. II, we introduce the problem formulation and quickly reiterate the mathematical background for using the split-Bregman approach in CT. Section III describes the set-up for the evaluation on simulated and measured preclinical in vivo μCT data. In Sec. IV we compare the combination of shearlets and TV to conventional algebraic reconstruction and to reconstruction with only one of these terms, for sparse-view data. These results are then discussed in Sec. V, where suggestions are also made for further research. Our conclusions are in Sec. VI.

II. PRELIMINARIES

Previously, we have developed the split-Bregman framework for regularized CT reconstruction [8], [12], [13]. We denote an ℓ_1-norm by $|.|_1$ and and ℓ_2-norm by $||.||_2$. The following minimization problem is solved:

$$\hat{\mathbf{x}} = \arg\min_{\mathbf{x}} E(\mathbf{x}) + \lambda||\mathbf{C}^{-1/2}(\mathbf{y} - \mathbf{W}\mathbf{x})||_2^2, \qquad (1)$$

with $\mathbf{x}$ the unknown reconstructed image, $E(\mathbf{x})$ the penalty term, λ the Lagrangian multiplier, a constant which determines

the amount of data-fitting and amount of regularization, $\mathbf{C}$ a prewhitening term, $\mathbf{y}$ the measured data and $\mathbf{W}$ the system matrix.

The penalty term $E(\mathbf{x})$ can include different regularizers. Previously, the ℓ_1-norm of the discrete gradient operator has already been used in anisotropic fasion [13], as well as a case where shearlets were used [8]. In this study, we will use a penalty term combining both:

$$E(\mathbf{x}) = \gamma_{TV}\left(|\nabla_x \mathbf{x}|_1 + |\nabla_y \mathbf{x}|_1\right) + \gamma_{SH}|\mathbf{Sx}|_1, \qquad (2)$$

with ∇ the discrete gradient operator, $\mathbf{S}$ the shearlet transform and constants γ_{TV} and γ_{SH} weighting the influence of the two components.

This cost function can be minimized by using Bregman iterations and variable splitting [12], effectively splitting the ℓ_1- and ℓ_2-norm into subproblems which are easier to solve [13]. This results in equations (3a) - (3g).

III. MATERIALS AND METHODS

A. Simulated data

Fan-beam data was simulated using MC-GPU v1.2 [14][1], a GPU-accelerated x-ray transport simulator. A high resolution phantom was built based on the work of the FORBILD group[2] (Fig. 1a). The resolution rods were simulated as containing air, surrounded by soft tissue. One $3.6864 \times 3.6864 \times 0.1395$ cm thick slice was generated, containing 8192×8192 voxels, to get sufficient subsampling in the holes with smallest diameter. The detector was simulated as a perfect detector with 100% efficiency, and consists of 296 elements with a pixel pitch of 0.14 mm, acquiring 360 uniformly spaced projection views over 2π. All data was generated using a 60 keV monoenergetic x-ray source with 10^8 photons per ray. The sinogram includes scattered photons.

B. Measured data

The X-O CT system (Gamma Medica Ideas, Northridge, California, USA) was used to obtain preclinical data of one in vivo contrast-enhanced mouse study. This flat-panel cone-beam system consists of a 1280×1120 detector with a 100 μm pixel pitch. The tube current is determined automatically during calibration to ensure that the dynamic range of the detector is optimally used. Fan-beam data were generated by retaining only the central detector row. 2048 projection views were obtained over 2π. A new dataset was generated from this projection data, by removing all but every 16th projection (128 views).

C. Data reconstruction and analysis

All datasets were reconstructed using 4 methods: SIRT, split-Bregman using anisotropic TV (SpBR-TV), split-Bregman using shearlets (SpBR-SH) and split-Bregman using both shearlets and anisotropic TV (SpBR-SHTV). In SpBR, Eq. 3a was solved using 30 iterations of conjugate gradient

[1]Freely available from http://code.google.com/p/mcgpu/
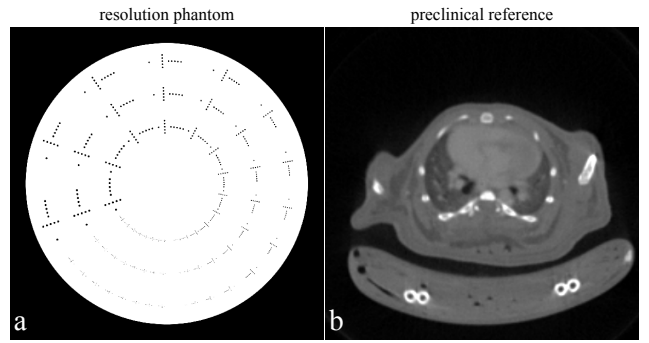[2]http://www.imp.uni-erlangen.de/phantoms/highcontrast/highcontrast.html

Fig. 1. Reference images for the simulated data (resolution phantom converted to 60 keV attenuation values) and the preclinical data (converged SIRT reconstruction of 2048 projection views).

on the normal equations. Matrix $\mathbf{W}$ was implemented as the 2D Distance Driven projector [15]. The shearlet transform $\mathbf{S}$ was implemented as previously implemented by Goossens et al. [16], based on the Meyer wavelet. Equations 3b-3d were implemented using soft-shrinkage [12]. Equations 3e-3g are trivial to solve. All regularized reconstructions converged and were stopped at iteration 20. All SIRT reconstructions were stopped when $||\mathbf{x}^{(i+1)} - \mathbf{x}^{(i)}||_2^2 / ||\mathbf{x}^{(i+1)}||_2^2 < 10^{-4}$.

The simulated data was reconstructed to a 256^2-grid with voxel pitch 0.16 mm, the preclinical data was reconstructed to a 256^2-grid with 0.13 mm voxel pitch. The diagonal elements of $\mathbf{C}$ (see Eq. 3a) were set to $c_{ii} = e^{-y_i}$ [17] with y_i the measured counts, serving as an estimator for the mean number of counts.

For each regularized reconstruction, parameter λ was empirically chosen, by reconstructing with different λ values and gradually making the search interval smaller, fine tuning the amount of denoising. This generally results in 5 to 10 reconstructions needed to determine a good λ value for the case of only one regularizer. When SH and TV were combined, γ_{SH} and γ_{TV} also had to be empirically determined. The parameter μ was always set to $0.585 \times \lambda$, which was empirically determined.

The peak signal-to-noise ratio (PSNR) was determined to objectively evaluate the preclinical images. The SIRT reconstruction of 2048 projection views was used as the reference high dose image (Fig. 1b).

IV. RESULTS

Figure 2 shows the resolution phantom reconstructed with the different methods, zoomed in to the low resolution part of the resolution phantom. some For SpBR-TV, noise patches become apparent in the heavily denoised image ($\lambda = 600$), compared to less denoising ($\lambda = 4000$). However, a slight increase in resolution can be noted when only a small amount of denoising is applied. Furthermore, the rods are shaped irregularly and are not perfectly round.

In the SH reconstruction, denoising with a low λ factor does not eliminate all noisy patches in between of the rods. The resolution increases when less denoising is used, also increasing the noise in the background. However, when SH and TV are combined ($\gamma_{SH} = 1.0$ and $\gamma_{TV} = 0.45$), round

$$\mathbf{x}^{(i+1)} = \arg\min_{\mathbf{x}} \frac{\lambda}{2}||\mathbf{C}^{-1/2}(\mathbf{y} - \mathbf{W}\mathbf{x})||_2^2 + \frac{\mu}{2}||\mathbf{d}_{TV,x}^{(i)} - \nabla_x(\mathbf{x}) - \mathbf{b}_{TV,x}^{(i)}||_2^2 \tag{3a}$$
$$+ \frac{\mu}{2}||\mathbf{d}_{TV,y}^{(i)} - \nabla_y(\mathbf{x}) - \mathbf{b}_{TV,y}^{(i)}||_2^2 + \frac{\mu}{2}||\mathbf{d}_{SH}^{(i)} - \mathbf{S}\mathbf{x} - \mathbf{b}_{SH}^{(i)}||_2^2$$

$$\mathbf{d}_{TV,x}^{(i+1)} = \arg\min_{\mathbf{d}} |\mathbf{d}|_1 + \frac{\mu}{2}||\mathbf{d} - \nabla_x\mathbf{x}^{(i+1)} - \mathbf{b}_{TV,x}^{(i)}||_2^2 \tag{3b}$$

$$\mathbf{d}_{TV,y}^{(i+1)} = \arg\min_{\mathbf{d}} |\mathbf{d}|_1 + \frac{\mu}{2}||\mathbf{d} - \nabla_y\mathbf{x}^{(i+1)} - \mathbf{b}_{TV,y}^{(i)}||_2^2 \tag{3c}$$

$$\mathbf{d}_{SH}^{(i+1)} = \arg\min_{\mathbf{d}} |\mathbf{d}|_1 + \frac{\mu}{2}||\mathbf{d} - \mathbf{S}\mathbf{x}^{(i+1)} - \mathbf{b}_{SH}^{(i)}||_2^2 \tag{3d}$$

$$\mathbf{b}_{TV,x}^{(i+1)} = \mathbf{b}_{TV,x}^{(i)} + (\nabla_x\mathbf{x}^{(i+1)} - \mathbf{d}_{TV,x}^{(i+1)}) \tag{3e}$$

$$\mathbf{b}_{TV,y}^{(i+1)} = \mathbf{b}_{TV,y}^{(i)} + (\nabla_y\mathbf{x}^{(i+1)} - \mathbf{d}_{TV,y}^{(i+1)}) \tag{3f}$$

$$\mathbf{b}_{SH}^{(i+1)} = \mathbf{b}_{SH}^{(i)} + (\mathbf{S}\mathbf{x}^{(i+1)} - \mathbf{d}_{SH}^{(i+1)}). \tag{3g}$$
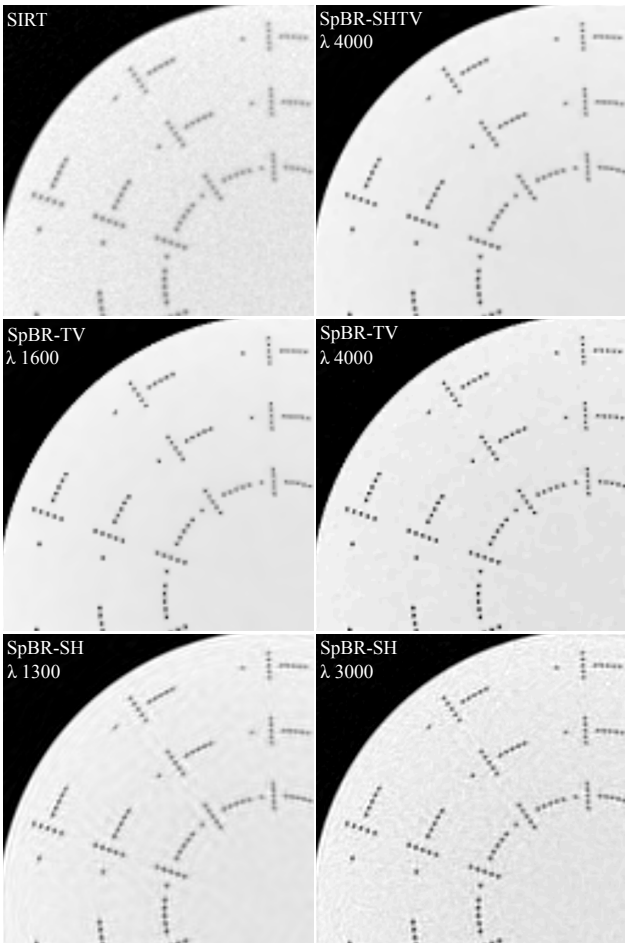

Fig. 2. Comparison of SIRT of noisy data, combined SH and TV (γ_{SH} = 1.0, γ_{TV} = 0.45), TV with low and high λ, SH with low and high λ. All images were normalized to the same window.

rods are achieved, whilst still perfectly minimizing the noise in the background.

Figure 3 compares SpBR-TV, SpBR-SH and SpBR-SHTV to the reference high-dose SIRT reconstruction in the case of measured preclinical data. Parameter λ was set to 2000 for SpBR-SHTV, with $\gamma_{SH} = 0.25$ and $\gamma_{TV} = 1.0$. Plotted on the right are the absolute difference images, each time between the reconstruction and the reference image. SIRT shows streaking artifacts when only 128 views are used. All regularized reconstructions lead to higher PSNR compared to SIRT.

The difference image for SpBR-TV shows some resolution loss at the edges of the animal bed and at the body contour, primarily at edges which are not mainly horizontally or vertically oriented. For SH, these edges are not visible. However, there are some streaking artifacts left, which could not be minimized with a different λ choice without sacrificing resolution. When SH and TV are combined, good denoising properties are obtained with a small amount of resolution loss. This is primarily visible at the sternum, where the spongious bone is more difficult to distinguish on SpBR-SHTV reconstructions than on SIRT or with TV alone.

V. DISCUSSION

Combining TV and SH regularization into one algorithm shows benefits for sparse-view CT imaging. Previous research has shown that shearlets do not lead to any form of piecewise-constant behavior, but on the other hand do not tend to approximate uniform regions as well as TV [8]. The preliminary results presented here show that a combination of both regularization terms combines the benefits of both SH as well as TV.

One tricky and very sensitive area is parameter selection in iterative algorithms. Next to determining λ empirically, there is now also the difficulty of weighing the contribution of SH against the contribution of TV with γ_{SH} and γ_{TV}. Special care has to be taken to not let TV overpower SH, as this will result in piecewise constant behavior. In theory, we would like to use shearlets to minimize the cost function in general, and use a little bit of TV to minimize the introduced artifacts, such as Gibbs phenomena next to jump discontinuities, or remaining streaking artifacts. We have shown that this works sufficiently in the case of preclinical data, although with a small loss of resolution. This may be due to parameter selection.

On the other hand, a larger γ_{TV} than γ_{SH} is needed when phantom data is reconstructed. Shearlets can not reconstruct
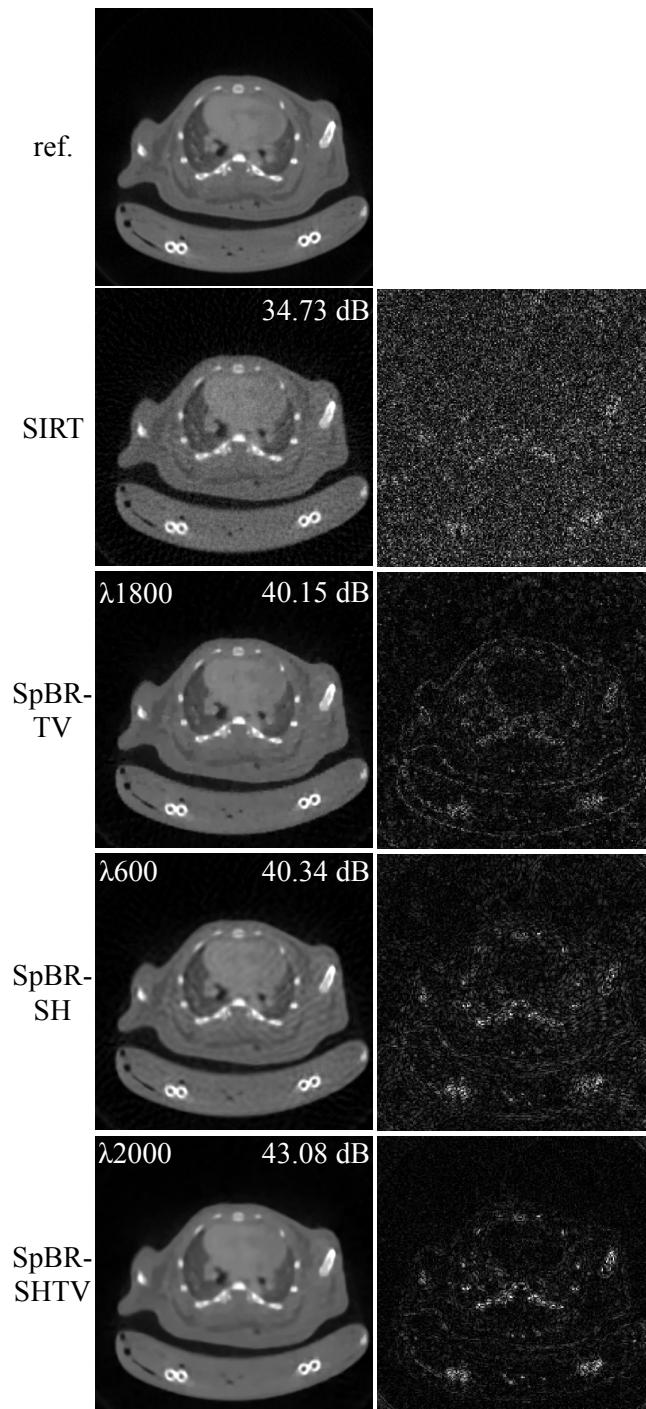
Fig. 3. Preclinical sparsified data reconstructed from 128 projection views with SIRT, SpBR-TV, SpBR-SH and SpBR-SHTV ($\gamma_{SH} = 0.25$, $\gamma_{TV} = 1.0$). All images were normalized to the same window. Difference is the absolute difference between reconstruction and reference.

the uniform areas in phantoms accurately, as was demonstrated with the resolution phantom in Fig. 2. However, these cases are not realistic when doing (pre)clinical measurements. Optimal selection of these parameters will be subject to future research, as well as task-based observer studies to determine if SpBR-SHTV has better diagnostic value than simple TV minimization.

VI. CONCLUSION

We have combined TV and shearlet minimization into one reconstruction algorithm, and have shown its benefits for sparse-view CT imaging in a proof-of-concept study. A small loss of resolution is apparent, probably due to suboptimal parameter selection.

REFERENCES

[1] D. Gutierrez and H. Zaidi, "Assessment of scatter for the micro-CT subsystem of the trimodality FLEX Triumph™ preclinical scanner," *Medical Physics*, vol. 38, no. 7, p. 4154, 2011.

[2] L. I. Rudin, O. Stanley, and E. Fatemi, "Nonlinear total variation based noise removal algorithms," *Physica D: Nonlinear Phenomena*, pp. 259–268, 1992.

[3] G. T. Herman and R. Davidi, "Image reconstruction from a small number of projections," *Inverse Problems*, vol. 24, no. 4, 2008.

[4] M. Lustig, D. Donoho, and J. M. Pauly, "Sparse MRI: The application of compressed sensing for rapid MR imaging," *Magnetic Resonance in Medicine*, vol. 58, no. 6, pp. 1182–1195, 2007.

[5] M. Defrise, C. Vanhove, and X. Liu, "An algorithm for total variation regularization in high-dimensional linear problems," *Inverse Problems*, vol. 27, no. 6, p. 065002, May 2011.

[6] G. Kutyniok and D. Labate, "Resolution of the Wavefront Set Using Continuous Shearlets," *Transactions of the American Mathematical Society*, vol. 361, no. 5, pp. 2719–2754, 2009.

[7] K. Guo, D. Labate, and W.-Q. Lim, "Edge analysis and identification using the continuous shearlet transform," *Applied and Computational Harmonic Analysis*, vol. 27, no. 1, pp. 24–46, 2009.

[8] B. Vandeghinste, B. Goossens, R. Van Holen, C. Vanhove, A. Pižurica, S. Vandenberghe, and S. Staelens, "Iterative CT reconstruction using shearlet-based regularization," *Proc. of SPIE*, pp. 1–7, 2012.

[9] A. Pižurica, J. Aelterman, F. Bai, S. Vanloocke, H. Quang Luong, B. Goossens, and W. Philips, "On structured sparsity and selected applications in tomographic imaging," *Proc. of SPIE Conference Wavelets and Sparsity XIV*, p. 81381D, 2011.

[10] L. He, T.-C. Chang, S. Osher, T. Fang, and P. Speier, "MR image reconstruction from undersampled data by using the iterative refinement procedure," *PAMM*, vol. 7, no. 1, pp. 1 011 207–1 011 208, Dec. 2007.

[11] J. Huang, S. Zhang, H. Li, and D. Metaxas, "Composite splitting algorithms for convex optimization," *COMPUTER VISION AND IMAGE UNDERSTANDING*, pp. 1–13, Sep. 2011.

[12] T. Goldstein and S. Osher, "The split Bregman method for L1 regularized problems," *SIAM Journal on Imaging Sciences*, vol. 2, no. 2, pp. 323–343, 2009.

[13] B. Vandeghinste, B. Goossens, J. De Beenhouwer, A. Pižurica, W. Philips, S. Vandenberghe, and S. Staelens, "Split-Bregman-based sparse-view CT reconstruction," *Proceedings of the 11th International Meeting on Fully 3D Image Reconstruction*, pp. 431–434, 2011.

[14] A. Badal and A. Badano, "Accelerating Monte Carlo simulations of photon transport in a voxelized geometry using a massively parallel graphics processing unit," *Medical Physics*, vol. 36, no. 11, p. 4878, 2009.

[15] B. de Man and S. Basu, "Distance-driven projection and backprojection in three dimensions." *Physics in Medicine and Biology*, vol. 49, no. 11, pp. 2463–2475, 2004.

[16] B. Goossens, J. Aelterman, H. Luong, A. Pižurica, and W. Philips, "Efficient design of a low redundant discrete shearlet transform," *Proc. of the 2009 Int. Workshop on Local and Non-Local approximation in Image Processing*, 2009.

[17] S. Ramani and J. Fessler, "A Splitting-Based Iterative Algorithm for Accelerated Statistical X-Ray CT Reconstruction." *IEEE Transactions on Medical Imaging*, Nov. 2011.